Electron states in α-quartz: A self-consistent pseudopotential calculation

James R. Chelikowsky and M. Schlüter
Bell Laboratories, Murray Hill, New Jersey 07974
(Received 21 December 1976)

Self-consistent pseudopotentials are used to investigate the electronic structure of α-quartz. We present calculations for the band structure, electronic density of states, optical response functions, pseudocharge densities, and x-ray emission spectra. We find excellent agreement between theory and experiment with respect to photoemission and uv absorption data. The chemical bonding present in α-quartz as determined from pseudocharge density contour maps is consistent with other theoretical calculations. The theoretical x-ray emission spectra, as obtained from an orthogonalized-plane-wave scheme, are compared with experimental data. The calculated silicon and oxygen K spectra agree very well with experiment; however, the Si $L_{2,3}$ spectrum exhibits substantial disagreement with the data. An explanation is proposed based upon the formation of amorphous elemental Si in SiO_2 during electron irradiation.

I. INTRODUCTION

In this paper, we shall present results of a self-consistent pseudopotential calculation for the electronic structure of SiO_2 in the form of α-quartz. While numerous theoretical investigations have been performed on SiO_2,[1-13] this is the first *realistic* study in that we combine a self-consistent-field (SCF) treatment of the valence electrons with an actual structural form of SiO_2. Previous theoretical studies have concentrated on empirical or semiempirical molecular-orbital schemes,[1-3,9] molecular-cluster calculations,[4-8,10] or *ad hoc* band structures based upon idealized forms of SiO_2.[11,12] Therefore, the previous theoretical approaches are deficient in several respects. For example, the molecular-orbital schemes and band-structure calculations are not self-consistent. They may, therefore, yield an incorrect description of ionicity or charge transfer. The molecular-orbital schemes have also been rather specialized and are consequently limited in their applicability.[9,12] Although the cluster calculations may be made self-consistent, a question may arise as to whether the size of the cluster is sufficient to accurately replicate the crystalline structure. In addition to the aforementioned lack of self-consistency, the band-structure calculations have been performed on an idealized structure; questions may therefore arise as to whether the idealized structure accurately reproduces the hybridization in actual forms of SiO_2.

Thus, while these approaches have been reasonably successful in presenting a consistent description of the chemical bonding in SiO_2, a comprehensive picture of the electronic structure for a realistic form of SiO_2 is still lacking. In addition, the motivation for a realistic treatment of SiO_2 is reinforced by the existence of several inconsistencies present in the interpretation of x-ray emission and optical spectra.[14]

The self-consistent pseudopotential method[15] eliminates many of the drawbacks present in the previous theoretical studies of SiO_2. In this method, the valence electrons are allowed to respond to a specified structural arrangement represented by a superposition of rigid ionic pseudopotentials. The pseudocharacter of the potentials, i.e., the elimination of core states, is determined by reproducing the valence eigenvalues and wave functions, away from the core region, as calculated by SCF atomic-structure techniques.[16] Once this procedure has been performed for the Si^{4+} and O^{6+} pseudopotentials, *no* other adjustments are made with respect to the potentials. Thus, the calculation involves no adjustable parameters fit to experimental data. With the removal of the core states, we may achieve fairly rapid convergence by a plane-wave basis. In this fashion, we avoid problems associated with other techniques. For example, no atomic configurations need be specified, and no problems arise with respect to the choice of minimal localized basis sets as we diagonalize a Hartree-Fock-Slater Hamiltonian in a plane-wave basis.

Besides the numerous theoretical studies on SiO_2, intensive experimental measurements have been carried out on this technologically important material. To briefly summarize, these experiments include measurements of photoemission spectra,[17-19] photoconductivity,[20] optical spectra,[2,21-23] x-ray emission and absorption spectra,[14,24-26] low energy loss spectra,[27] and Auger electron spectra.[28] In this respect, SiO_2 can serve as a "testing ground" for the various theoretical techniques available. We shall, therefore, endeavor to make comparisions between our theoretical results and experimental data whenever possible.

The paper is outlined as follows. In Sec. II, we

will discuss the calculational techniques involved in constructing the ionic pseudopotentials and in forming the resulting secular equation. In addition the theoretical procedures used in calculating the x-ray emission spectra will be discussed. In Sec. III, the theoretical results are compared to experiment, and in Sec. IV, we shall present some conclusions and summarize our results.

II. CALCULATIONAL TECHNIQUES

The inputs into our calculation include the crystal structure and the ionic pseudopotentials. The crystal structure may be obtained from x-ray data and the ionic potentials from atomic structure calculations. Since no adjustments in the potentials were made to fit experimental data, the calculational techniques described below are of a first-principles nature.

As discussed elsewhere,[29] SiO_2 occurs in many allotropic forms. With the exception of stishovite, all the forms are constructed from a tetrahedral configuration of SiO_4. In this arrangement, the silicons are bonded to four oxygens, and the oxygens to two silicons. The only difference between the various forms is the manner in which the tetrahedrons are linked together. Previous band calculations[11,12] have concentrated on idealized β cristobalite. This form of SiO_2 can be visualized by considering a diamond lattice, e.g., elemental Si, with an enlarged lattice constant and oxygens located at the bond sites between silicon atoms. However, the existence of such an idealized form of SiO_2 with a straight Si–O–Si bonding configuration has *not* been established,[29] and at present no experimental data, other than lattice parameters, exist on β cristobalite.

While β-cristobalite may be the simplest conceptual form of SiO_2, it does not correspond to the most common form of SiO_2 which is α-quartz. In α-quartz, which has hexagonal D_3^4 symmetry, the unit cell consists of three molecular units of SiO_2. For a full description of the crystal structure the reader is referred to Ref. 29. To briefly summarize the crystal parameters, the a-axis length is 9.29 a_0 (1 Bohr radius $a_0 = 0.529$ Å) and the c-axis length is 10.217 a_0. The Si–O bond length in this form of SiO_2 is approximately 3.0 a_0 and the O–O distance varies from 4.9 to 5.05 a_0. The bond angle in Si–O–Si is not 180° as in the idealized β-cristobalite, but is approximately 144°. This fact is significant in determining hybridization effects.[7]

With respect to the crystalline potential we may write

$$V(\vec{r}) = \sum_{m,\alpha} V_i^{\alpha}(\vec{r} - \vec{R}_m - \vec{\tau}_\alpha) + V_{HX}(\vec{r}), \tag{1}$$

where V_i^{α} is the ionic pseudopotential for the αth atomic species, V_{HX} is the screening potential in the Hartree-Fock-Slater sense,[30] and the sum is over lattice vectors $\vec{R}_m$ where $\vec{\tau}_\alpha$ gives the position of the αth ion in the unit cell.

The plane-wave basis set used to diagonalize the Hamiltonian may be expressed as

$$\psi_{\vec{k}}(\vec{r}) = \frac{1}{\sqrt{\Omega}} \sum_{\vec{G}} a_{\vec{G}}(\vec{k}) \exp[i(\vec{k}+\vec{G})\cdot\vec{r}], \tag{2}$$

where Ω is the crystal volume, and the sum extends over reciprocal-lattice vectors $\vec{G}$. The coefficients $a_{\vec{G}}$ are found by a diagonalization of the secular equation.

In general, the ionic pseudopotentials are nonlocal[31] and we may write

$$V_i(\vec{r}) = \sum_{l=0}^{\infty} P_l^{+} V_i^{l}(\vec{r}) P_l, \tag{3}$$

where P_l is a projection operator which projects out the lth component of angular momentum present in the wave functions. For the case at hand, cluster calculations indicate[7,8,10] only s and p orbitals are significant in these valence wave functions. Therefore, we may restrict the sum in Eq. (3) to only the $l=0$ and $l=1$ terms.[31]

In the case of Si, the potential may be expressed solely in terms of a local pseudopotential, i.e., $V_i(\vec{r}) = V^i(|\vec{r}|)$ independent of l. This approach has been found to be highly accurate via both bulk and surface calculations performed on elemental Si.[30] However, in the case of oxygen this is not the case. Since there exist no $l=1$ components in the oxygen core states, no cancellation will occur for valence p states.[31] This problem has so far prevented accurate pseudopotential calculations from being carried out on oxide compounds.[31] However, the recent success of nonlocal pseudopotential calculations[32] and self-consistent pseudopotential calculations[30] suggest that the approach might yield an accurate ionic pseudopotential for oxygen.

For Si^{4+} the Fourier coefficients of the pseudopotential required for a solution of the secular equation may be obtained from

$$V_i^{\mathrm{Si}}(q) = (a_1/q^2)[\cos(a_2 q) + a_3]\exp(a_4 q^4), \tag{4}$$

where the a_i are given in Table I. This potential when self-consistently screened will yield the atomic eigenvalues of Si as calculated by SCF techniques.[16] In addition, the resulting pseudo-wave-functions were constructed such that the wave functions maxima for the pseudo $3s$ and $3p$ states correspond to those of the SCF atomic wave functions.

With respect to O, a nonlocal potential of the

TABLE I. Ionic pseudopotential parameters as defined in Eqs. (4) and (7). The O^{6+} parameters are for the local part of the pseudopotential. The units are such that if q is entered in atomic units (a.u.) then $V(q)$ is in Ry. The normalization volume is the atomic volume, $\Omega_a = 84.8$ a.u.

	Si^{4+}	O^{6+}
a_1	−1.829	−1.8265
a_2	0.7907	1.80
a_3	−0.3520	2.00
a_4	−0.018 07	•••

form

$$V_i^{\mathrm{O}}(r) = V_s(r) + P_1^{\dagger}\,[V_p(r) - V_s(r)]P_1 \tag{5}$$

was constructed. The potentials V_s and V_p were designed to reproduce the valence eigenvalues for the $2s$ and $2p$ states respectively, and the pseudo-wave-functions were matched to the actual wave functions[16] away from the core region.[30,31]

The form of V_s and V_p in real space was chosen to be

$$V_i^{l}(r) = -\frac{2Z}{r}\tanh(r) + A_l \exp\left(\frac{-r^2}{R_l^2}\right). \tag{6}$$

This form of the potential has the advantages of being simple and containing only two adjustable parameters. It correctly obeys the asymptotic behavior: $V_i^l(r\to\infty) = -2Z/r$. The parameters were taken to be $A_0 = -4.0$ Ry, $A_1 = -6.5$ Ry, and $R_0 = R_1 = 1.4a_0$ (atomic units will be used throughout the paper). As expected the p-well term is considerably deeper than the s well because of the absence of $l=1$ states within the core.

The required Fourier transform of the oxygen ionic pseudopotential, for the local part of the potential, V_s, was numerically determined from Eq. (6) and accurately fit to the following analytic expression:

$$V_s^{\mathrm{O}}(q) = (a_1/q^2)\{1 + \exp[a_2(q - a_3)]\}^{-1}; \tag{7}$$

the values of the a_i are given in Table I. The required matrix elements for the nonlocal part of the potential $P_1^{\dagger}(V_p - V_s)P_1$ may be expressed as

$$\langle \vec{q}\,|\,P_1^{\dagger}(V_p - V_s)P_1\,|\,\vec{q}'\rangle = (12\pi/\Omega_a)\cos(\theta_{\vec{q},\vec{q}'}) \times \frac{A_1 - A_0}{4\sqrt{qq'}}\pi R^2 \times \exp[-\tfrac{1}{4}R^2(q^2+q^{2\prime})]I_{3/2}(\tfrac{1}{2}R^2qq'), \tag{8}$$

where $I_{3/2}(x)$ is a modified spherical Bessel function,[33] Ω_a is the atomic value, and $\theta_{\vec{q},\vec{q}'}$ is the angle between the vectors $\vec{q}$ and $\vec{q}'$.

In the Hartree-Fock-Slater Hamiltonian the screening potential consists of two terms: a Hartree potential V_H determined from Poisson's equation, and an exchange potential V_X determined from the cube root of the charge density. The required matrix elements for V_H are given by

$$V_H(\vec{q}) = (4\pi/|q|^2)\rho(\vec{q}), \tag{9}$$

where $\rho(\vec{q})$ is the Fourier coefficient of the valence charge density. For V_X we take a local exchange term of the form

$$V_X(\vec{r}) = -6\alpha(3/8\pi)^{1/3}[\rho(\vec{r})]^{1/3}, \tag{10}$$

with $\alpha = 0.8$. This value of α was used for both the atomic and bulk calculations. To calculate the required matrix elements a Fourier transform of the cube root of the charge density was performed. This was accomplished by evaluating the charge density on a fine grid over the unit cell, approximately 800 grid points, taking the cube root at each point and then performing the summation

$$\rho_{\vec{q}}^{(1/3)} = \frac{1}{N}\sum_i [\rho(\vec{r}_i)]^{1/3}\exp(-i\vec{q}\cdot\vec{r}_i), \tag{11}$$

where N is the number of grid points $\vec{r}_i$. This yields

$$V_X(\vec{q}) = -6\alpha(3\pi^2)^{1/3}\rho_{\vec{q}}^{(1/3)}. \tag{12}$$

With the above expressions for the matrix elements, the secular equation may be written

$$|H_{\vec{G},\vec{G}'}(\vec{k}) - E(\vec{k})\delta_{\vec{G},\vec{G}'}| = 0, \tag{13}$$

where

$$H_{\vec{G},\vec{G}'}(\vec{k}) = (\vec{k}+\vec{G})^2\delta_{\vec{G},\vec{G}'} + \sum_{\alpha}[V_L^{\alpha}(|\vec{G}-\vec{G}'|) + \langle\vec{k}+\vec{G}\,|\,V_{NL}^{\alpha}(\vec{r})\,|\,\vec{k}+\vec{G}'\rangle] \times S^{\alpha}(\vec{G}-\vec{G}') + V_H(\vec{G}-\vec{G}') + V_X(\vec{G}-\vec{G}').$$

The V_L^{α} refers to the local contributions of the ionic pseudopotentials from Eqs. (4) and (7) and V_{NL}^{α} refers to the nonlocal correction from Eq. (8). The structure factor for the αth atomic species is denoted by $S_{\alpha}(\vec{G})$.[31]

Self-consistency was accomplished by a direct iteration process. To initiate the cycle, the screening potential V_{HX} was constructed from atomic potentials. With this "starting" potential the Hamiltonian was diagonalized at two special $\vec{k}$ points.[34,35] In the diagonalization process, approximately 150 plane waves were used to expand the wave functions; an additional 200 waves were incorporated by a perturbation scheme devised by Löwdin.[31] Once the wave functions at the special $\vec{k}$ points have been determined, an accurate val-

ence charge density is then used via Eqs. (9) and (12) to calculate a new potential. The diagonalization process is repeated and again a potential is created from the resulting valence-charge density. The cycle is carried out until essential agreement is found between the "input" and "output" screening potentials.[30] The iteration procedure was carried out until the screening potential was converged to within 0.01 Ry. For this convergence, the eigenvalues are stable to within 0.1 eV.

In order to establish an accurate description of the electronic density of states, the Hamiltonian was diagonalized at 16 $\vec{k}$ points in the irreducible part of the Brillouin zone. The results were then convoluted by a broadening function with a width at half-maximum of 0.5 eV. The same $\vec{k}$-point grid was used to evaluate the imaginary part of the dielectric function

$$\epsilon_2(\omega) = \frac{4\pi^2 e^2 \hbar}{3m^2\omega^2} \sum_{v,c} \int_{BZ} \frac{2}{(2\pi)^3} d\vec{k} |M_{c,v}|^2 \times \delta(\omega_{cv}(\vec{k}) - \omega), \quad (14)$$

where the sum extends over band indices for the conduction (c) and valence (v) bands, $|M_{c,v}|^2$ is the absolute squared dipole matrix element between the bands and $\hbar\omega_{cv}$ is the energy separation between them. If constant matrix elements are used then $\epsilon_2(\omega)$ corresponds to a joint density of states.

To analyze in detail the x-ray emission spectrum we have calculated the imaginary part of the dielectric function corresponding to transitions from valence states to core-hole states. In this procedure, the pseudo-wave-functions from Eq. (2) are first orthogonalized to all core states. The core wave functions may be expressed as

$$|b_t^\alpha\rangle = \frac{1}{\sqrt{N}} \sum_m \exp[i\vec{k}\cdot(\vec{R}_m + \vec{\tau}_\alpha)]\, a_t(\vec{r} - \vec{R}_m - \vec{\tau}_\alpha), \quad (15)$$

where N is the number of cells in the crystal and the a_t are core orbitals.[16] The orthogonalized wave functions are then given by

$$|\phi_{\vec{k}}\rangle = |\psi_{\vec{k}}\rangle - \sum_{t,\alpha} \langle b_t^\alpha | \psi_{\vec{k}}\rangle |b_t^\alpha\rangle. \quad (16)$$

The required matrix elements are given by

$$M_{vt} = \langle b_t^\alpha | \nabla | \psi_{\vec{k}}^v\rangle - \sum_{t'} \langle b_t^\alpha | \nabla | b_{t'}^\alpha\rangle \langle b_{t'}^\alpha | \psi_{\vec{k}}^v\rangle \quad (17)$$

where the transition involves a core-hole in the t-core state and an electron in the valence band labeled v. This technique, explained in detail elsewhere,[36] has been quite successful in analyzing core to conduction band transitions in lead salts. In that case, it was found that the orthogonalization procedure was crucial in obtaining accurate matrix elements.

III. RESULTS

In Fig. 1, the band structure for α-quartz is displayed along high symmetry lines in the hexagonal Brillouin zone. With three molecular units of SiO_2 in the unit cell of α-quartz, we find 24 occupied valence bands. A group theoretical assignment has not been performed on the bands of α-quartz. Therefore, we shall label the bands in ascending order with $\Gamma(1)$ referring to the lowest valence band at Γ and $\Gamma(24)$ referring to the top of the valence band at Γ. Possible band crossovers have been omitted in Fig. 1; they are not of importance for the discussion below.

The computed band gap is indirect, $M(24) - \Gamma(25)$, and is equal to 9.2 eV in magnitude. This result is in excellent agreement with photoconductivity experiments on amorphous SiO_2 in which the gap is measured to be 8.9 eV.[20] While the photoconductivity measurements were performed on amorphous quartz, the similarity between the reflectivity spectra of amorphous SiO_2 and α-quartz is quite striking and indicates the overall band structure of the two should be very similar.[20,21] The existence of an indirect gap is also compatible with reflectivity data which exhibit no strong structure below 10 eV.[21,23] Our computed band gap of 9.2 eV should be contrasted with that calculated for β-cristobalite[11] for which a mixed basis set was used. The calculated band gap was only about 6.0 eV resulting in an error of nearly 3 eV as compared to experiment. The discrepancy probably arises from the idealized form of SiO_2 and the lack of self-consistency (correct-charge transfer) in this calculation.

The band masses obtained from our calculation are, however, in qualitative accord with the estimates obtained from the β-crystobalite calculation. The conduction band minimum from Fig. 1 is roughly free-electron-like with an effective mass of $m_c^* \approx 0.3 m_e$. This is to be compared with an estimated mass of $m_c^* \approx 0.5 m_e$ from Ref. 11 and that obtained by analogy with other insulators.[11,37] The hole mass at the valence-band maximum we estimate to be $m_v^* \approx (5-10) m_e$. The hole mass is fairly anisotropic, but our estimate is consistent with the β-cristobalite results. Experimentally,[17] a fairly heavy hole mass is expected because of the narrow width of the levels near the valence band edge. It has been suggested that the heavy mass could lead to the lattice trapping of low energy holes, and that this could account for the positive charging of SiO_2 under ionizing radiation.[20]

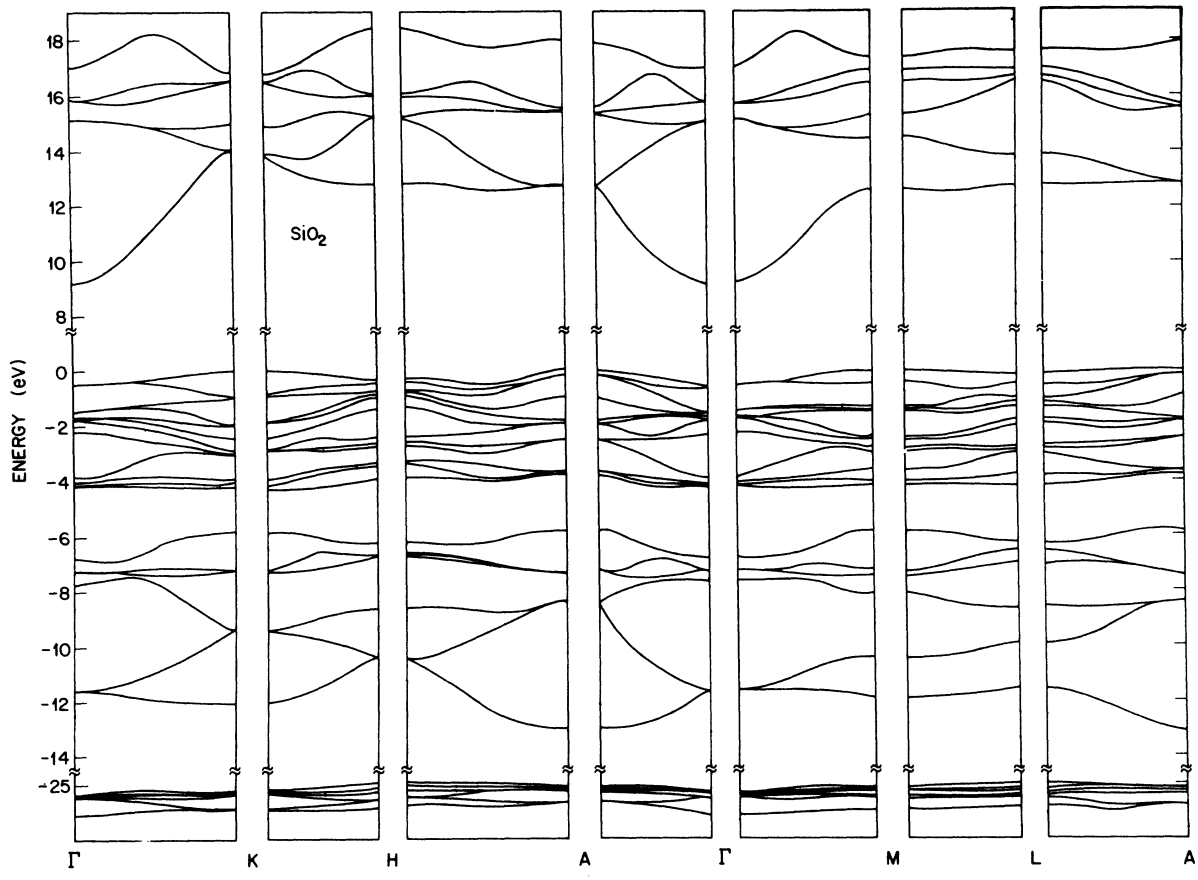

FIG. 1. Band structure of α-quartz.

In Fig. 2, the calculated density of states for α-quartz is presented and compared to the experimental results of ultraviolet and x-ray photoemission spectroscopy[17,18] on amorphous quartz. Also, listed in Table II are the calculated and experimental features observed in the spectra. On the basis of pseudocharge density analysis we divide the density of states into three general regions: oxygen ($2p$) nonbounding states, oxygen ($2p$)–silicon ($3s, 3p$) bonding states and oxygen ($2s$) corelike states.

The top part of the valence band, from the valence-band maximum (which is taken to be the zero reference) to approximately −5 eV, is predominantly composed on nonbonding oxygen p-like orbitals. This conclusion is based upon the pseudocharge density behavior for this energy region which is displayed in Figs. 3 and 4. As can be observed from the charge density, p-like orbitals are localized on the oxygen and are *not* oriented along the bonding directions. Unlike idealized β-cristobalite, α-quartz has a bond angle different from 180° and thus some hybridization of the orbitals is allowed. In amorphous SiO_2, the experimental "nonbonding peak," is a bit narrower than theoretically calculated for α-quartz.[17,18] This result is consistent with measurements obtained on amorphous and crystalline forms of Ge and Si: the amorphous p-like peak is narrower than the corresponding crystalline peak.[38] Besides the difference in peak width, the theoretical structure exhibits some fine structure (labeled in Fig. 2 by A, B, C) not present in the experimental spectra. This structure has been examined via a charge density map for each region. We find that the uppermost peak (A) is of a more "nonbonding" nature than the lower peak (C). This conclusion is based on the observation that the charge configuration in case (A) is localized out of the O–Si–O bonding plane to a greater extent than the charge density in case (C).

The region from −5.5 to −13.0 eV consists of O–Si bonding orbitals as indicated in Figs. 3 and 4. The region shows two structures, also indicated by experiment, which correspond to orbitals involving oxygen p states and silicon p states (−7.0 eV) and silicon s states (−12 eV). The distinction of the two peaks with respect to the silicon s-p character is illustrated in Figs. 3 and 4: the upper peak labeled D has significantly less

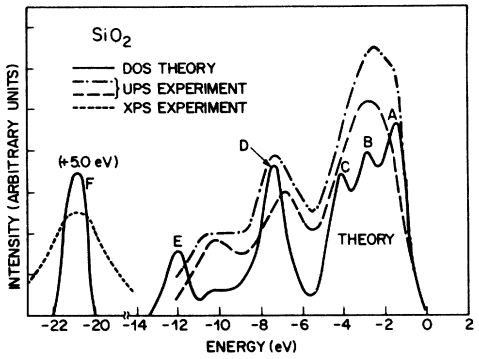

FIG. 2. Calculated density of states (DOS) for α-quartz (full line). Ultraviolet-photoemission (UPS) data (dashed line, Ref. 18; dashed-dotted line, Ref. 17) and x-ray-photoemission (XPS) data for the oxygen 2s level (dotted line, Ref. 17) for amorphous SiO_2 are superimposed. The calculated oxygen 2s level had to be shifted by +5eV to line up with experiment. The peaks labeled *A*, *B*, *C*, *D*, *E*, and *F* are discussed in the text.

charge at the silicon site than does peak *E*. This result is indicative of more *p*-character residing in the *D* peak.

The lowest valence bands correspond to O (2*s*) states as illustrated in Fig. 3 where the charge density for peak *F* is displayed. As found in the case of β-cristobalite the O (2*s*-2*p*) hybridization is quite small.[11] This has also been found to be the case in cluster calculations.[7] Thus, although the calculated placement of the oxygen 2*s* orbitals is lower than experiment by approximately 5 eV, the relatively small error in the binding energy of about 20% for these states should *not* affect the quantitative agreement with experiment of the upper valence bands. In fact, some studies of

TABLE II. Electronic density of states features. The energies are in eV and the valence band maximum is referenced to zero.

Feature	Experiment Ref. 17	Experiment Ref. 18	Theory
Nonbonding oxygen (2*p*)	−2.5	−2.5	−2.5
Bonding oxygen (2*p*)–silicon (3*p*)	−6.5	−7.0	−7.0
oxygen (2*p*)–silicon (3*s*)	−10.0	−10.5	−12.0
Oxygen (2*s*)	−20.5	−21.0	−25.5

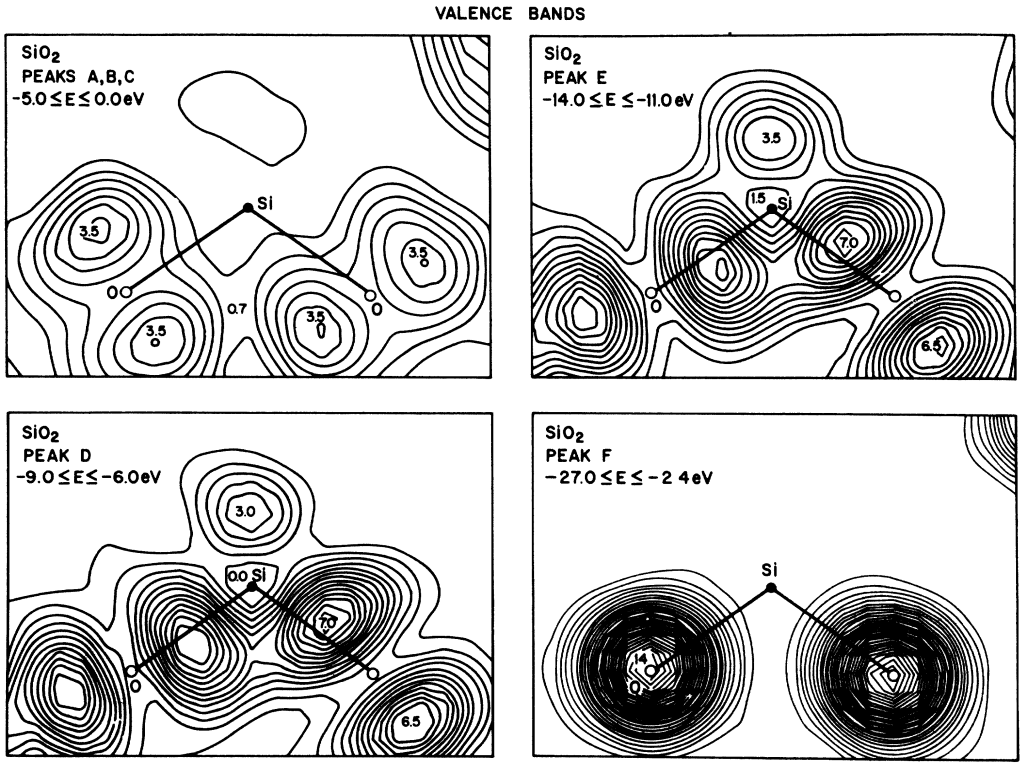

FIG. 3. Valence pseudocharge densities for the electronic density of states features in α-quartz. The charge densities are plotted in the O–Si–O bonding plane and are arbitrarily normalized. The peaks and energy regions are displayed in Fig. 2.

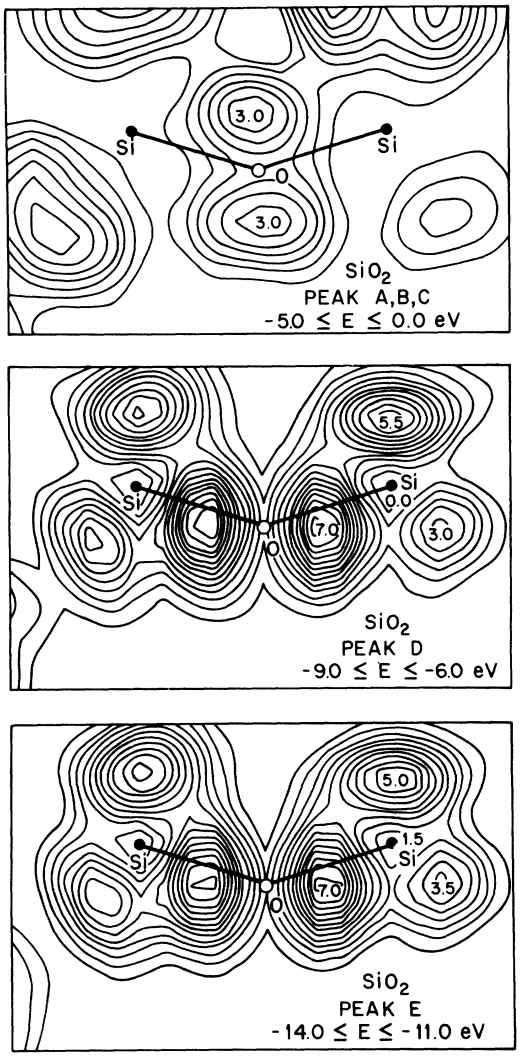

FIG. 4. Valence pseudocharge densities for the electronic density of states features in α-quartz. The charge densities are plotted in the Si–O–Si bonding plane and are arbitrarily normalized. The peaks and energy regions are displayed in Fig. 2.

SiO_2 have neglected the presence of the O ($2s$) corelike states altogether.[12]

In Fig. 5, we present the total valence charge density for α-quartz. Our calculation indicates a fairly ionic compound with a majority of charge localized on the oxygen sites. Cluster calculations have suggested an atomic population in the Si–O bond of Si(+0.78)O(−0.78) and for Si–O–Si a population of Si_2(+0.37)O(−0.74).[7] It is not possible to quantify our pseudocharge densities in such a fashion, since a significant amount of charge is located in the Si–O bonds.

In Fig. 6, the calculated imaginary part of the dielectric function $\epsilon_2(\omega)$ and the joint density of

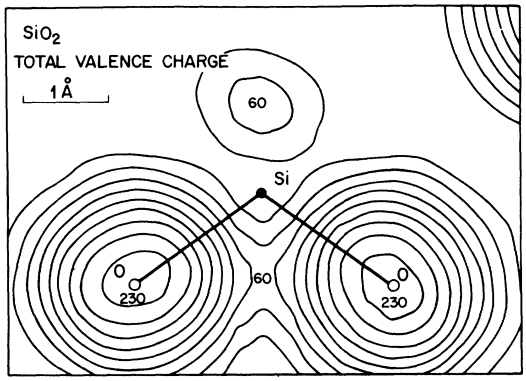

FIG. 5. Total valence pseudocharge density for α-quartz displayed in the O–Si–O bonding plane. The charge is normalized to 48 electrons per unit cell.

states are compared with experimentally determined uv $\epsilon_2(\omega)$ data. The measured spectrum exhibits strong peaks at 10.4, 11.7, 14.0, and 17.3 ev.[14,21-23] The first peak has been proposed as excitonic in origin through temperature-dependent studies.[14,22] In fact, a simple estimate of the excitonic binding energy in SiO_2 yields a value of 1.3 eV in agreement with the separation of the first two reflectivity peaks.[9] The theoretically calculated joint density of states does not exhibit any structure below 15 eV, in disagreement with the experimental spectrum. However, when dipole matrix elements are introduced significant structure appears at 11 and 13 eV. It is found, as in the case of β cristobalite,[11] that the lowest direct-interband transitions are dipole forbidden. This shifts the onset of absorption to higher en-

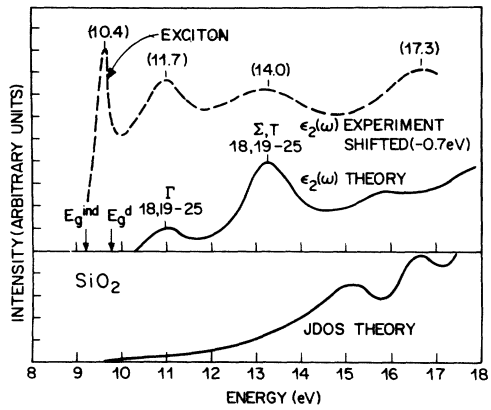

FIG. 6. Calculated joint density of states (JDOS) for direct transitions in α-quartz (bottom). The inclusion of dipole matrix elements yields $\epsilon_2(\omega)$ (top). Positions of the direct and indirect gap as well as locations in $\vec{k}$ space of prominent transitions are indicated. An experimental $\epsilon_2(\omega)$ spectrum from Ref. 14 shifted by −0.7 eV is superimposed.

ergies by about 1.2 eV. Both peaks at 11 and 13 eV involve transitions between states of oxygen $2p$ and oxygen $3s$ character. The origin of these transitions in the Brillouin zone is labeled in Fig. 6. (The labels Σ and T correspond to the Γ-M and Γ-K directions in the Brillouin zone, respectively.) The higher energy structure in the calculated ϵ_2 near 17 eV is attributed to arise from volume contributions. Figure 7 displays the pseudocharge density character for the valence to conduction band transitions occurring between $\Gamma(18,19) \rightarrow \Gamma(25)$. While the conduction states also contain significant silicon p and d character, the oxygen $2p$ valence states localize the transitions essentially on the oxygen sites. Therefore, the exciton in SiO_2, which we attribute to the sharp peak at 10.4 eV in the uv data, is of *anionic character*. This assignment of the 10.4 and 11.7 eV peaks with $O(2p) \rightarrow O(3s)$ is in agreement with previous speculations. In particular, to account for the striking similarity between the uv spectra of fused and crystalline quartz, it has been proposed that the dominant transition in SiO_2 must be between oxygen orbitals.[2]

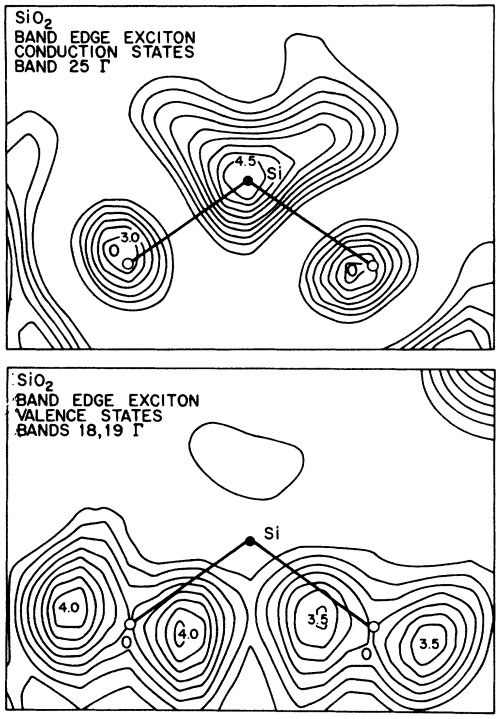

FIG. 7. Pseudocharge densities for the states involved in the lowest allowed optical transitions in α-quartz. The top part of the figure displays the (unoccupied) charge density of the Γ(25) conduction state and the bottom part of the figure displays the (occupied) charge density of the Γ(18,19) valence states. The normalization is arbitrary and the plane shown contains the O–Si–O bonds.

For a complete comparison between theory (with no excitonic effects) and experiment we have also displayed in Fig. 6 the experimental imaginary part of the dielectric function from Ref. 14. The experimental spectrum has been shifted by −0.7 eV to line it up with theory. In spite of this shift which is less than 10% of the band gap, the agreement is quite good.

In Fig. 8, we compare experimental x-ray emission data[14] with the theoretical spectra. This is the first quantitative comparison of this kind for α-quartz. Previous calculations have concentrated on molecular clusters,[6-8,10] or β-cristobalite.[11,12]

No core-relaxation and electron-hole screening effects are considered in calculating the spectra. While the former effects are globally taken into consideration by adjusting the core–valence-band transition energy, the latter effects are expected to be small in large-gap insulators such as SiO_2. This approximation is invalid and yields very poor results for x-ray *absorption* spectra which are known to show strong excitonic effects.[12]

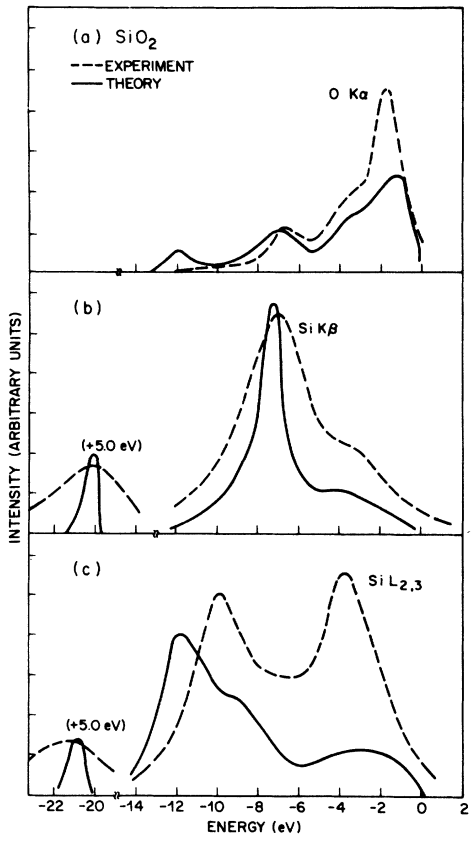

FIG. 8. Experimental (full lines, Ref. 14) and calculated (broken lines) x-ray emission spectra of SiO_2. The experimental spectra are lined up to a common energy scale as discussed in the text.

With respect to the experimental x-ray emission spectra of Fig. 8, the Si $K\beta$ and Si $L_{2,3}$ results are brought to a common energy scale as proposed in Refs. 11 and 14 using atomic spectroscopic data, while the relative position of the oxygen $K\alpha$ spectrum is taken according to Ref. 11 (which differs from Ref. 14).

With the exception of the Si $L_{2,3}$ spectrum we generally find very good agreement between the experimental and theoretical x-ray emission spectra. Because of dipole selection rules, the oxygen $K\alpha$ spectrum samples oxygen p-states in the valence bands. Therefore, the major contribution to this spectrum arises from the nonbonding oxygen $2p$-like orbitals near the valence-band maximum; other contributions arise from bonding states at somewhat higher binding energies. We find no emission from the oxygen $2s$ states which are dipole forbidden. The Si $K\beta$ spectrum analogously samples Si p-states which are found in the "bonding region" of the spectrum. In addition, significant emission is observed and calculated (note the correct relative intensity) from the oxygen $2s$ levels. This emission originates from oxygen $2s$ levels sufficiently overlapping with Si core levels. Thus, no cross-over transitions[7] need to be invoked to explain the satellite oxygen $2s$ emission peak which also appears in the Si $L_{2,3}$ spectrum.

The calculated Si $L_{2,3}$ spectrum should sample Si s or d character. Our results are in poor agreement with experiment. The measured spectrum shows an almost symmetric two-peak structure. However, the theoretical spectrum indicates strong emission only on the higher-binding-energy part of the spectrum corresponding to Si $3s$-character contributions. The lower-binding-energy peak in the experimental spectrum occurs in a region dominated by oxygen p states. Even though some emission is theoretically predicted in this region, the disagreement in intensity between experiment and theory is significant. The discrepancy is even more surprising if one considers the excellent quantitative agreement of the K spectra, photoemission, and uv reflectivity.

Early calculations on molecular clusters suggested that Si $3d$ character might be responsible for the second peak.[6] However, this suggestion has been criticized on the grounds that the basis set used was not correctly chosen.[7] More-recent calculations in agreement with the present calculations have, in fact, yielded little Si $3d$ character in the upper part of the valence band.[7,8] Furthermore, relaxation effects which have also been suggested[6,7] as an explanation to the disagreement of theory with experiment can be ruled out because of the good agreement observed for the K spectra.

At present, while we have no quantitative explanation for the discrepancy, we strongly believe that the existence of elemental Si in SiO_2 is responsible for the second peak. For example, amorphous Si is formed during the process of electron bombardment while taking the x-ray emission spectrum. This process, termed electron impact desorption, is well known in plasma physics to destroy quartz tubings. In addition, electron irradiation effects in the Auger spectra of SiO_2 have recently been investigated.[28] It was observed that the SiO_2 surface became enriched in elemental silicon even for rather small electron beam currents. The presence of elemental silicon should also be seen in the Si $K\beta$ spectrum. In fact, it may well be responsible for the increased oscillator strength at lower binding energies observed in the spectrum.

IV. CONCLUSION

We have investigated the electronic structure of SiO_2 in the form of α-quartz by means of self-consistent pseudopotentials. Calculations were presented for the band structure, electronic density of states, optical response functions, pseudocharge densities, and x-ray emission spectra. The calculations present a comprehensive investigation of an actual form of SiO_2. No adjustable parameters based upon experimental data (other than the lattice parameters) entered the calculation.

We were able to accurately reproduce the experimentally determined band gap, optical spectrum and photoemission spectrum. The calculated band gap was 9.2 eV and found to be indirect. The lowest optical transitions were calculated to be anionic in character and are dominated by O $(2p)-$O $(3s)$ transitions. With respect to the photoemission spectrum we obtain quantitative agreement for the valence states within a Rydberg of the valence-band maximum. Our placement for the core-like O $(2s)$ states is approximately 20% in error compared to experiment with the theoretical result too tightly bound.

The bonding configuration we find for α-quartz is compatible with previous cluster calculations and band-structure calculations for idealized β-cristobalite. We find the lowest valence states, which correspond to oxygen $2s$ states, do not significantly hybridize with the oxygen $2p$ states. The remainder of the valence band consists of silicon-oxygen bonding states and less tightly bound oxygen "nonbonding" p states. Some crystal-field or bond-angle induced hybridization effects are also found for these states.

We have also examined x-ray emission spectra.

The calculated spectra were obtained in an orthogonalized-plane-wave scheme and compared to experiment. While the Si and O K spectra agree well with experiment, the Si $L_{2,3}$ spectrum shows substantial differences. Our calculations in agreement with cluster calculations on SiO_2 do not support the conclusion that Si 3d states are present to any significant extent in the valence bands. Therefore Si 3d states cannot be responsible for the experimentally observed results. We suggest that the discrepancy arises from the formation of elemental (amorphous) Si during electron irradiation of SiO_2.

In conclusion, we hope our calculations will provide a theoretical basis upon which satisfactory interpretations may be made for *all* experimental data on α-quartz.

ACKNOWLEDGMENTS

We would like to thank P. H. Citrin, W. Heiland, J. D. Joannopoulos, R. Pollak, and J. E. Rowe for helpful conversations.

[1]A. F. Ruffa, Phys. Status Solidi 29, 605 (1968).
[2]M. H. Reilly, J. Phys. Chem. Solids 31, 1041 (1970).
[3]I. V. Abarenkov, A. V. Amosov, V. F. Bratsev, and D. M. Yudin, Phys. Status Solidi 2, 865 (1970).
[4]A. J. Bennett and L. M. Roth, J. Phys. Chem. Solids 32, 1251 (1971).
[5]A. J. Bennett and L. M. Roth, Phys. Rev. B 4, 2686 (1971).
[6]G. A. D. Collins, D. W. J. Cruickshank, and A. Breeze, J. Chem. Soc. Faraday Trans. II 68, 1189 (1972).
[7]T. L. Gilbert, W. J. Stevens, H. Schrenk, M. Yoshimine, and P. S. Bagus, Phys. Rev. B 8, 5988 (1973).
[8]T. A. Tossell, D. J. Vaughan, and K. H. Johnson, Chem. Phys. Lett. 20, 329 (1973).
[9]A. F. Ruffa, J. Non-Cryst. Solids 13, 37 (1973/74).
[10]K. L. Yip and W. B. Fowler, Phys. Rev. B 10, 1400 (1974).
[11]P. M. Schneider and W. B. Fowler, Phys. Rev. Lett. 36, 425 (1976).
[12]S. T. Pantelides and W. A. Harrison, Phys. Rev. B 13, 2667 (1976).
[13]A preliminary account of this work was published by the authors in Solid State Commun. 21, 381 (1977).
[14]G. Klein and H. U. Chun, Phys. Status Solidi B 49, 167 (1972), and references therein.
[15]For example, see J. A. Appelbaum and D. R. Hamann, Phys. Rev. B 8, 1777 (1973); and M. Schlüter, J. R. Chelikowsky, S. G. Louie, and M. L. Cohen, *ibid.* 12, 4200 (1975).
[16]F. Herman and S. Skillman, *Atomic Structure Calculations* (Prentice-Hall, Englewood Cliffs, N.J., 1963).
[17]T. H. DiStefano and D. E. Eastman, Phys. Rev. Lett. 27, 1560 (1971).
[18]H. Ibach and J. E. Rowe, Phys. Rev. B 10, 710 (1974).
[19]J. E. Rowe, Appl. Phys. Lett. 25, 576 (1974).
[20]T. H. DiStefano and D. E. Eastman, Solid State Commun. 9, 2259 (1971).
[21]H. R. Philipp, Solid State Commun. 4, 73 (1966).
[22]K. Platzöder, Phys. Status Solidi 29, K63 (1968).
[23]H. R. Philipp, J. Phys. Chem. Solids 32, 1932 (1971).
[24]D. W. Fischer, J. Chem. Phys. 42, 3814 (1965).
[25]A. Mattson and R. C. Ehlert, Adv. X-Ray Anal. 9, 471 (1966).
[26]O. A. Ershov and A. P. Lukirskii, Fiz. Tverd. Tela 8, 2137 (1966) [Sov. Phys. Solid State 8, 1699 (1967)].
[27]A. Koma and R. Ludeke, Phys. Rev. Lett. 35, 107 (1975).
[28]S. Thomas, J. Appl. Phys. 45, 161 (1974).
[29]R. W. G. Wyckoff, *Crystal Structures* (Interscience, New York, 1965), and references therein.
[30]See, M. Schlüter, J. R. Chelikowsky, S. G. Louie, and M. L. Cohen, Phys. Rev. Lett. 34, 1385 (1975), and Ref. 15.
[31]M. L. Cohen and V. Heine, Solid State Phys. 24, 37 (1970).
[32]See for example, J. R. Chelikowsky and M. L. Cohen, Phys. Rev. B 14, 556 (1976), and references therein.
[33]M. Abramowitz and I. A. Stegun, *Handbook of Mathematical Functions* (Dover, New York, 1964), p. 443.
[34]A. Baldereschi, Phys. Rev. B 7, 522 (1973).
[35]D. J. Chadi and M. L. Cohen, Phys. Rev. B 8, 5747 (1973).
[36]G. Martinez, M. Schlüter, and M. L. Cohen, Phys. Rev. B 11, 660 (1975).
[37]J. W. Hodby, in *Polarons in Ionic Crystals and Polar Semiconductors*, edited by J. T. Devreese (North-Holland, Amsterdam, 1972); U. Rössler, Phys. Status. Solidi 42, 345 (1970).
[38]L. Ley, S. Kowalczyk, R. Pollak, and D. A. Shirley, Phys. Rev. Lett. 29, 1088 (1972).